



Evening Temperature Rises on Valley Floors and Slopes: Their Causes and Their Relationship to the Thermally Driven Wind System

C. DAVID WHITEMAN* AND SEBASTIAN W. HOCH

Department of Meteorology, University of Utah, Salt Lake City, Utah

GREGORY S. POULOS⁺

National Center for Atmospheric Research,[#] Boulder, Colorado

(Manuscript received 1 May 2008, in final form 3 October 2008)

ABSTRACT

At slope and valley floor sites in the Owens Valley of California, the late afternoon near-surface air temperature decline is often followed by a temporary temperature rise before the expected nighttime cooling resumes. The spatial and temporal patterns of this evening warming phenomenon, as seen in the March/April 2006 Terrain-Induced Rotor Experiment, are investigated using a widely distributed network of 51 surface-based temperature dataloggers. Hypotheses on the causes of the temperature rises are tested using heavily instrumented 34-m meteorological towers that were located within the datalogger array. The evening temperature rise follows the development of a shallow temperature deficit layer over the slopes and floor of the valley in which winds blow downslope. Background winds within the valley, freed from frictional deceleration from the earth's surface by this layer, accelerate. The increased vertical wind shear across the temperature deficit layer eventually creates shear instability and mixes out the layer, creating the observed warming near the ground. As momentum is exchanged during the mixing event, the wind direction near the surface gradually turns from downslope to the background wind direction. After the short period of warming associated with the mixing, ongoing net radiative loss causes a resumption of the cooling.

1. Introduction

As part of the Terrain-Induced Rotor Experiment (T-REX) of March and April 2006 (Grubišić et al. 2008), temperature dataloggers were installed on lines oriented along and across the axis of the deep Owens Valley on the east side of the Sierra Nevada (Fig. 1). Temperature time series from these loggers exhibited temperature decreases after local sunset. But, in many instances, the temperature would rise again before beginning a more general nighttime decline. The purpose

of this paper is to investigate the anomalous temperature rises by determining their characteristics and the distribution of these characteristics in time and space. Then we formulate and test hypotheses concerning their origin by using case studies of events that were observed with heavily instrumented meteorological towers located within the temperature datalogger array.

2. The Owens Valley

Owens Valley, located between the north-northwest-to-south-southeast-oriented Sierra Nevada and Inyo-White Mountain chains, is one of the deepest valleys in the United States. Between Lone Pine and Bishop, California, where our instruments were located, the Sierra Nevada on the west side of the valley has a largely uninterrupted mountain ridgeline, with a mean elevation of 4000 m MSL. On the east side of the valley, the Inyo-White Mountains have a mean elevation of 3000 m. The valley floor between these mountain chains has a mean elevation of 1200 m, so that the valley is 1800–2800 m

* Certified Consulting Meteorologist (CCM).

⁺ Current affiliation: Clipper Windpower Development, Inc., Denver, Colorado.

[#] The National Center for Atmospheric Research is sponsored by the National Science Foundation.

Corresponding author address: C. David Whiteman, CCM, Department of Meteorology, University of Utah, 135 S 1460 E, Rm. 819, Salt Lake City, UT 84112-0110.
E-mail: dave.whiteman@utah.edu

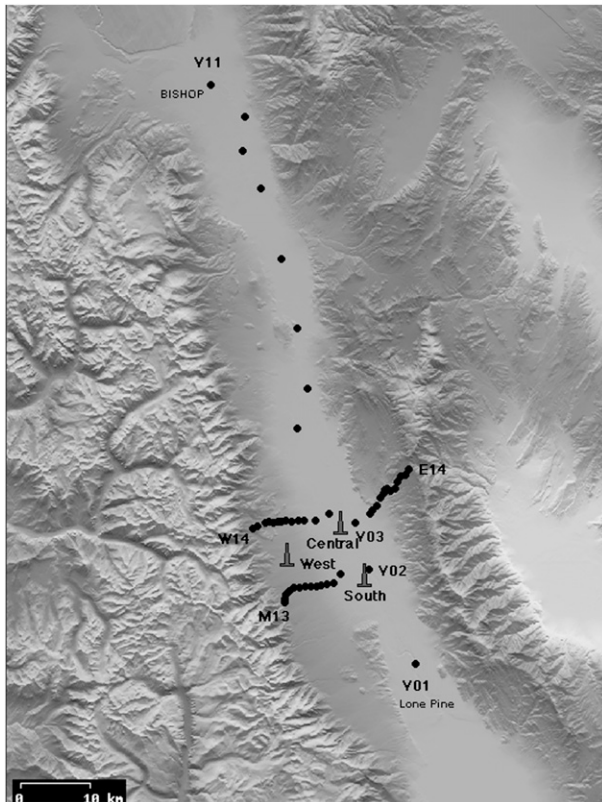


FIG. 1. HOBO sites (dots) and ISFF tower locations in the Owens Valley (from NCAR map server).

deep. The valley has a semiarid climate. The west side of the valley floor at the foot of the southern Sierra Nevada has a gentle incline at the lower elevations, with coarse sandy soil and widely dispersed shrubs; the east side is steep and rocky, with little vegetation except for widely dispersed evergreen trees at the upper elevations.

3. Instrumentation

a. The temperature datalogger lines

Temperature dataloggers (HOBO¹ Pro Temp/Ext Temp) were placed at 51 sites on the lines indicated in Fig. 1. Whiteman et al. (2000) described the characteristics of these loggers and their suitability for meteorological research. The thermistor temperature sensors used in these loggers were installed on steel fence posts in un-aspirated 6-plate radiation shields at heights of 1.3 m AGL. Temperature data were sampled and stored in the loggers at 5-min intervals during the 2-month-long experiment. One line, the valley line, ran up the Owens

Valley floor from Lone Pine to Bishop; the instruments on this line were numbered V01–V11. A second or west line ran perpendicular to the valley axis up the west (Sierra Nevada) slope of the Owens Valley through Independence, California, with instruments numbered W01–W13. A third or east line was located on the opposite side of the Owens Valley and ran up the east (Inyo–White Mountains) slope, with instruments numbered E01–E14. A fourth or Manzanar line ran up the west (Sierra) slope of the Owens Valley through Manzanar, California, approximately 10 km to the south of the west line, with instruments numbered M01–M13. The Manzanar line was installed in a segment of the valley where there was no major pass to the west. In contrast, Kearsarge Pass was located west of Independence, uphill of the west line.

HOBOs were placed at preselected elevations, with elevation spacing increasing with altitude above the valley floor. This first criterion provided spacing that allowed good height resolution at the lowest elevations, where vertical temperature gradients were expected to be a maximum. The secondary selection criterion was used to ensure that the measured temperatures at the elevations chosen were representative of the bulk valley atmosphere rather than local microclimates on the slope. Where possible, HOBOs were placed on convex terrain (i.e., on ridges rather than gullies or other declivities) away from bushes and rock outcrops. The upper segments of the Manzanar and west lines were on ridges, while the lower segments were on a broad and rather uniform alluvial slope. The lower segment of the Manzanar line was placed alongside a gravel road in a broad and shallow declivity.

b. The embedded tall towers

Three (central, west, and south) heavily instrumented integrated surface flux facility (ISFF) towers, installed and operated by the National Center for Atmospheric Research (NCAR), provided supplementary meteorological data. These 34-m towers (Fig. 1) were located inside the network of temperature dataloggers. The central and south sites were on the valley floor on slopes of about 0.2° in an area of dense brush, with an average height of 0.8 m. The west tower was on a slope of 3.25° in an area of sparse brush and rocky ground. The three towers had (1) Campbell CSAT3 sonic anemometers at 5, 10, 15, 20, 25, and 30 m; (2) Krypton hygrometers at 5 and 30 m; (3) temperature/relative humidity sensors at 5, 15, and 30 m; and (4) a barometer at 1-m height. The sonic anemometers were operated at 60 Hz, allowing for detailed evaluation of momentum and heat fluxes. Four-component radiation and soil heat flux, soil temperature, and soil moisture sensors were located adjacent to each of the towers. Radiometers were installed at the

¹ A registered trademark of Onset Computer Corporation, Bourne, Massachusetts.

2-m level. Three additional sonic anemometers were installed at the 1-, 2-, and 3-m levels at the central tower in April (more dataset information is available online at <http://www.eol.ucar.edu/rtf/projects/trex/isff/>).

It is important to note that the 34-m towers were tall enough to extend through shallow evening near-surface wind and temperature layers to sample the background up- or downvalley flows in the main bulk of the valley atmosphere. Descriptions of the relationships between near-surface wind and temperature structure and the higher-level background flows can thus be made solely from tower data.

4. Warming episode definition

The unusual feature observed initially in the HOBO data and illustrated in Fig. 2 is a temporary evening rise in temperature. The rise follows a period of normal late afternoon and early evening temperature decrease and is, in turn, followed by the reestablishment of the normal nighttime temperature decrease. The temperature rises are unusual for their singularity (i.e., they are often a single rise rather than a series of short-term oscillations), duration (usually 0.5–3 h), and regular occurrence within a few hours after sunset. This rise thus differs from the multiple, small amplitude rises of 0.05 to ~0.5-h periodicity associated with temperature oscillations (e.g., Stone and Hoard 1989; Monti et al. 2002) that accompany drainage flow pulsations on slopes (e.g., van Gorsel 2003) or from small tributaries (e.g., Porch et al. 1989). As a first step in investigating the phenomenon, a computer program was written to identify the times and locations where rises were present in the observational period using 5-min-averaged data. The program began by identifying relative temperature minima and maxima in the time period from 1700 to 2140 Pacific standard time (PST) on each day of the 2-month long T-REX field experiment. The program then searched for rises on these days in three time windows: 1700–2010, 1700–2055, and 1700–2140 PST. For each time window, the absolute minimum was selected from the relative minima and then the largest relative maximum occurring after the absolute minimum was identified. The use of three time windows improved the performance of the algorithm for finding the large, singular rises of interest, especially when weak temperature oscillations accompanied strongly declining temperatures late in the 1700–2140 PST period. The largest rise in the three time windows was then selected, and the characteristics of the rise were determined, including the temperature rise (ΔT ; °C), the elapsed time for the rise (Δt ; h), and the area of the rise as determined by integration (A ; °C h). In addition, we determined the

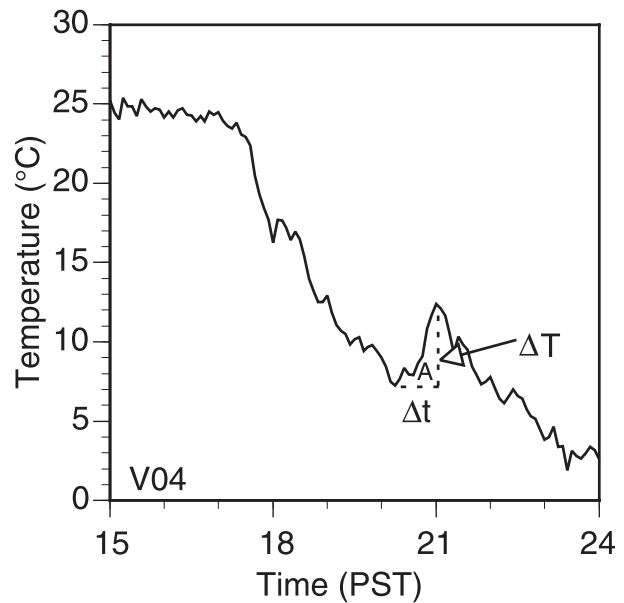


FIG. 2. Example warming episode at site V04 on 19 Apr 2006 illustrating the temperature rise ΔT (°C), duration Δt (h), and integrated area A (°C h).

dates and times when the rises formed at the widely distributed HOBO and tower sites, thus gaining information on both the temporal and spatial distribution of the phenomenon. It is important to note that the algorithm used to identify rises was able to find rises at most sites and dates, but many of these were simply the most energetic of the normal drainage flow temperature oscillations. In a later step [section 5a(1)], we attempt to exclude simple drainage flow oscillations by selecting for further analysis only the events for which $A \geq 0.75^\circ\text{C h}$. The purpose of these analyses was to objectively characterize the rises as a first step in developing hypotheses regarding mechanisms for their formation.

5. Characteristics of warming episodes

a. Warming events at the temperature datalogger sites

Of the 51 dataloggers, 47 had nearly complete records for the 67 days from 23 February through 30 April 2006. Analyses were therefore focused on these dataloggers. The 67-day period was somewhat unusual climatologically, with many passing synoptic-scale disturbances, high-wind events, and mountain waves (Grubišić et al. 2008).

1) FREQUENCY OF OCCURRENCE AND CHARACTERISTICS OF WARMING EPISODES

The potential number of site days was 3149 (47 sites \times 67 days). Occasional missing data at some sites reduced

the number of site days to 2949. Temperature rises were present on all site days; however, in many cases, the rises were small and represented normal slope flow oscillations, changes in cloud cover, or other disturbances to the local surface energy balance. The rises, durations, and areas of the rises tended to have lognormal distributions (Figs. 3a–c), with high frequencies of small rises, durations, and areas. Previous studies on slopes (see section 4) found evening velocity and temperature oscillations with 15–30-min periodicities and temperature oscillation magnitudes of about 1°C. Valley and basin velocity oscillations investigated by Tyson (1968) and Doran and Horst (1981) had maximum periodicities of 45–90 min. No temperature data were reported, but if these velocity oscillations were associated with temperature oscillations of 1°C, they would produce temperature rise areas $< \sim 0.5\Delta T\Delta t = 0.75^\circ\text{C h}$. Thus, to restrict our analysis to the longer-term, larger temperature rises of interest, we confined further analyses to temperature rises with $A \geq 0.75^\circ\text{C h}$. Using this cutoff, the rise characteristics become more normally distributed (the black histograms in Figs. 3a–c). A total of 544 site days (18% of the 2949 site days) exhibited such rises. Averaged over all such site days, temperature rises were 2.5°C, and durations were 1.1 h. Rises were observed at 10 or more sites on 25 of the 67 days and at 15 or more sites on the following days: 25 February: 2, 8, 10, 15, and 28 March; and 2, 17, and 28 April. Rises of this magnitude were entirely absent at all sites on 26 and 27 February, and on 9, 17, 18, and 27 March; these dates can be generally characterized as stormy or high-wind days.

The onset of the temperature rise occurs after local sunset. The onset time is quite variable, however, typically occurring between 1830 and 2100 PST. The variability in the timing of the temperature rises is probably related to the day-to-day differences in synoptic conditions. The phasing of slope and valley flows is well known to be sensitive to synoptic conditions (see, e.g., Barr and Orgill 1989; Doran 1991; Whiteman 2000).

2) BEST DAYS AND SITES FOR WARMING EPISODES

The 544 rises were distributed throughout the experimental period and were seen with varying frequencies at different datalogger sites. Mean values of A for each of the days of the experiment, as averaged over all temperature dataloggers for which $A \geq 0.75^\circ\text{C h}$ on that date, are shown in Fig. 4. Average areas exceeded 2°C h on 5, 8, and 22 March and on 2 and 16 April.

Figure 5a shows the number of temperature rises having $A \geq 0.75^\circ\text{C h}$ as a function of elevation for sites on the four HOBO lines. Mean values of temperature rise for these cases, the mean duration of the rises, and the rise areas are shown in Figs. 5b–d, respectively.

The *number of rises* was generally highest at the lowest elevations. Site W01, sites on the valley floor line, sites at the middle altitudes on the west line, sites at the lowest altitudes on the Manzanar line, and sites M10 and M08 on the Manzanar line had the highest frequency of temperature rise events. Only a small number of events occurred on the east line.

The *temperature rises* ΔT were generally largest at the lowest elevations, including all sites on the valley line, the lowest site on the west line (W01), sites W05 and W06, and several sites in the vicinity of M10. There was a general tendency for the temperature rises to decrease with altitude.

The *temperature rise durations* Δt were generally in the range of 0.75–1.5 h. Durations were somewhat shorter at all sites located near the valley floor at altitudes between 1100 and 1200 MSL and on the Manzanar line between 1550 and 1650 m MSL. The small number of events on the east line and on the upper west line decrease the statistical significance of the characteristics determined there.

The *areas of the temperature rises* A are proportional to the product of temperature rise and temperature rise duration. The variation of A with altitude is thus generally similar to the variation of temperature rise with altitude, since warming duration varies little with altitude. In the lowest couple of hundred meters above the valley floor on the valley, Manzanar and west lines, A decreases with altitude. Interestingly, above this altitude, there is little variation of A with altitude on the Manzanar line because of an inverse relationship between temperature rise and temperature rise duration. The largest values of A are seen at W05 and W06.

b. Warming events at the tower sites

Evening warming events were present at the towers as well as at the HOBO temperature datalogger sites. HOBOs closest to the three towers were V03 (central tower), M08 (west tower), and V02 (south tower). Because the towers were instrumented at multiple heights, the towers provided an opportunity to determine how the temperature rise characteristics changed with height above ground at the two valley floor and one sidewall tower sites (Fig. 6). Figure 6a presents the number of rises observed at different heights on the towers. The low number of rises below 5 m at the central tower is the result of the reduced period of record at these heights. The magnitude of the temperature rises (Fig. 6b) decreased with height, the duration showed little variation with height (Fig. 6c), and the area (Fig. 6d) decreased with height on the towers.

Additional data from meteorological instruments at the many levels on the towers provided a more

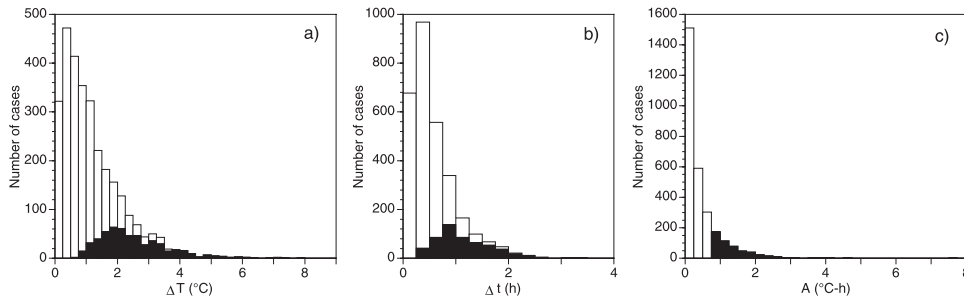


FIG. 3. Distribution (white bars) of HOBO (a) temperature rise ΔT ($^{\circ}\text{C}$), (b) duration Δt (h), and (c) area A ($^{\circ}\text{C h}$). Black bars are distributions for rises having $A \geq 0.75^{\circ}\text{C h}$.

extensive dataset, which allowed the testing of hypotheses regarding the causes of the phenomenon. That testing is accomplished in the following section.

6. Case studies at the towers

In this section, we describe three evening warming cases to demonstrate that the underlying cause of the temperature rises is the shear-driven interaction of the katabatic slope flows with accelerating overlying along-valley flows. All three cases were typical events in terms of their temperature rise areas (Fig. 4) and all were selected after mid-April, when additional sensors were operated at heights below 5 m on the central tower. The case studies were selected to illustrate evening temperature rises occurring with a background downvalley flow (17 April), an upvalley flow (19 and 24 April), and an event where rises occurred at different times at two of the tower sites (24 April). For these case studies, data are shown for

the south and central towers. The west tower, located on a small hill, usually exhibited weaker temperature rises than the other two towers (more on this in section 7b).

a. 17 April 2006

On the evening of 17 April, temperature rises with areas greater than 0.75°C h occurred at most sites on the west line, except for W07, W10, and W11, and at most sites on the valley line, except for V08, V10, and V11. The largest area, 3.83°C h , was seen at W01. Areas never exceeded 0.34°C h on the east line, except for 0.78°C h at E01.

Data at the central and south towers averaged in 5-min intervals (Fig. 7) showed that strong evening warming events occurred there as well as at the HOBO sites. Figure 7a indicates the early evening surface radiating temperatures (solid lines) and 5-m (dashed lines) air temperatures for the two towers. The surface radiating temperatures were obtained from pyrgeometer

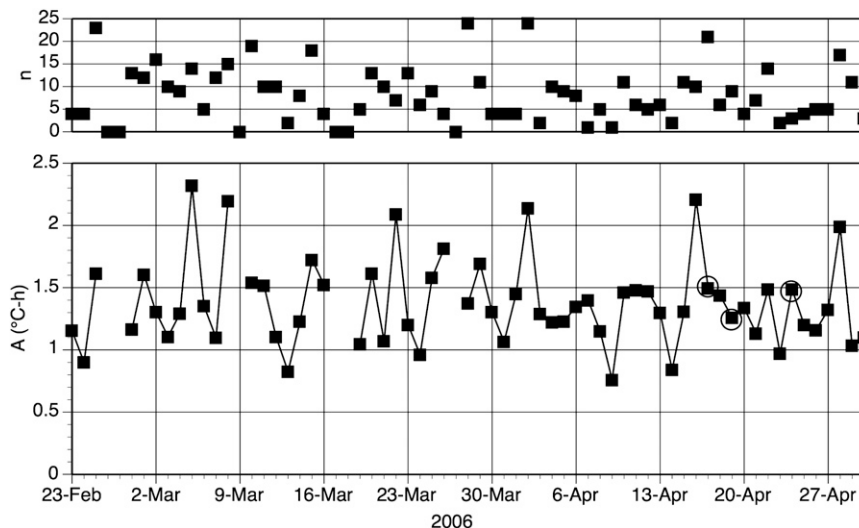


FIG. 4. Mean values of A as a function of day of year. Points are averages of all HOBO sites with $A \geq 0.75^{\circ}\text{C h}$ for that day. (top) The number of sites n meeting this criterion are indicated. (bottom) Missing data points are days when no sites met the criterion. The circled points identify the case study dates.

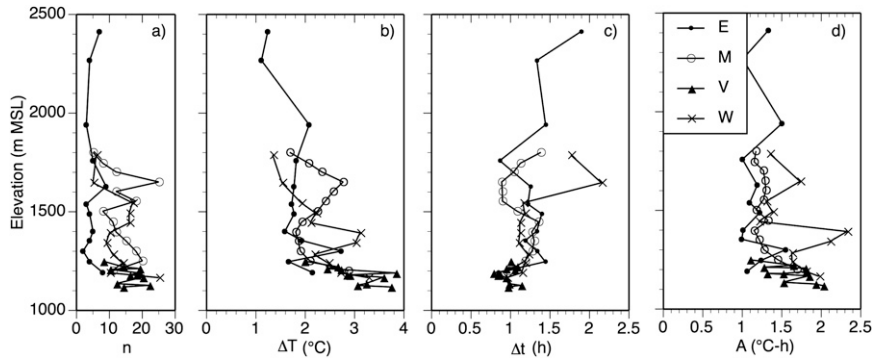


FIG. 5. (a) Number of temperature rises, and mean values of (b) temperature rise, (c) rise duration, and (d) rise area as a function of elevation for the east (E), Manzanar (M), valley (V), and west (W) HOBO lines, as averaged at each site for all days having $A \geq 0.75^\circ\text{C h}$ at that site.

measurements using the Stefan–Boltzmann law and assuming a surface emissivity of 1. The 7°C rise at the central tower was 0.75 h in duration, while the 4°C rise at the south tower was 0.67 h in duration. Wind speed (Fig. 7b) and direction (Fig. 7c) changes were closely related to the temperature evolution. Up until 1730 PST, winds at both towers were blowing down the valley axis (i.e., generally from the north-northwest) at 4 m s^{-1} . Before sunset the daytime downvalley wind began to decrease to $2.0\text{--}2.5 \text{ m s}^{-1}$. Immediately following sunset, winds shifted into a westerly downslope direction. Downslope flows, with some variability in direction, persisted until the warming episode began at 2040 PST. At that time, wind speeds increased and shifted back to downvalley, with the rise ending at 2115 PST.

The surface energy budget components are shown in Fig. 7d, using the sign convention that fluxes directed toward the surface, whether from the ground or atmosphere, are positive. Because the 5-min-average latent and sensible heat fluxes were quite variable, they were smoothed with a five-point moving average to produce the curves in the figure. Latent heat flux was near-zero, consistent with the dry climate. Ground heat

flux reversed before sunset and steadily rose to a nighttime level of several tens of watts per square meter. The ground heat flux was determined from a flux plate measurement at 0.05-m depth and was corrected for flux divergence in the soil above the plate using the mean temperature of this layer and the measured soil heat capacity. Net radiation is a mirror image of the surface radiating temperature during the period of temperature rise and fall because, after sunset, the net radiation is driven primarily by outgoing radiation, which is a function of surface radiating temperature. Incoming longwave radiation, measured during the experiment, exhibited a slow decrease during the evening period (not shown), indicating the slowly cooling atmosphere. Net radiation is thus seen as a proxy measurement of the surface radiating temperature during the period of temperature rise and fall, with the presence of the temperature rise and its subsequent fall indicated by a rise and fall of net radiation.

A downward-directed sensible heat flux of $10\text{--}30 \text{ W m}^{-2}$ occurred during the cooling period before the temperature rise. The warming episode is marked by the rapid increase in downward turbulent sensible heat flux triggered by an increased wind shear at the top of

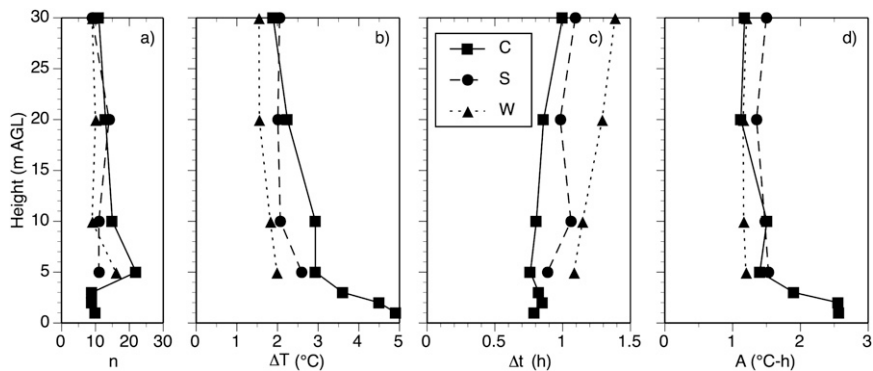


FIG. 6. As in Fig. 5, but for the central (C), south (S), and west (W) towers.

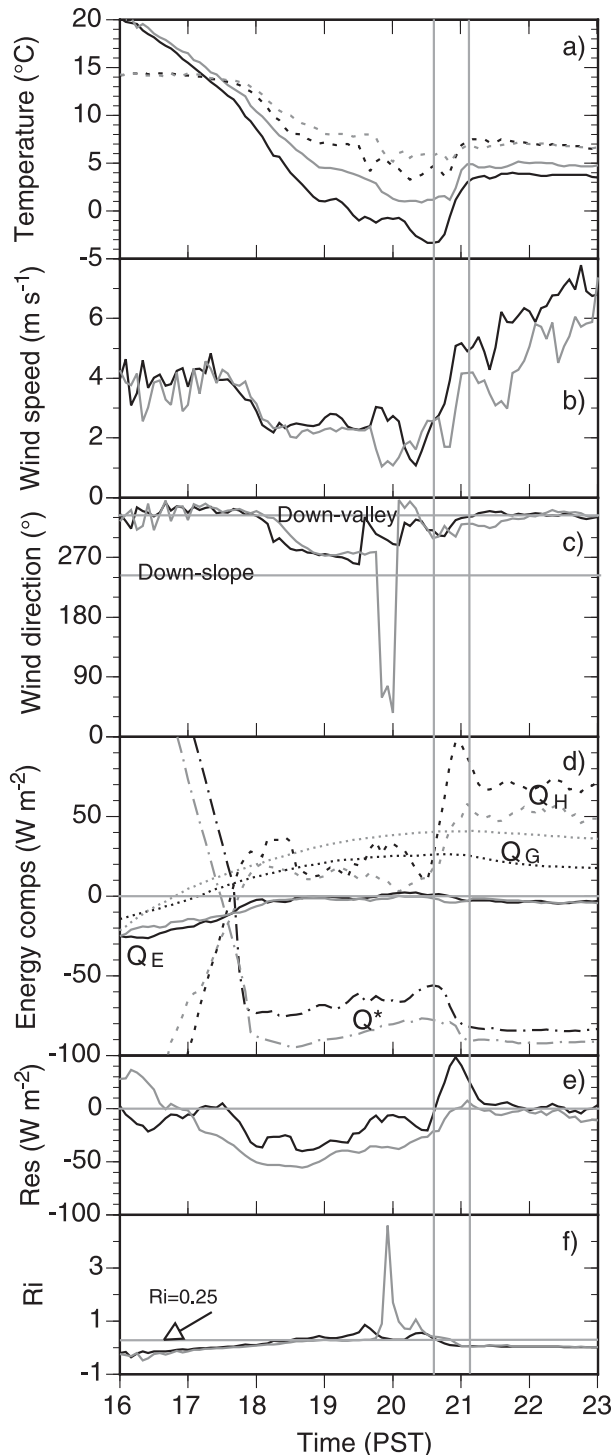


FIG. 7. Meteorographs from the central (black) and south (gray) towers for 17 Apr 2006. (a) Surface radiating temperature (solid lines) and 5-m air temperature (dashed lines); (b) 5-m wind speed; (c) 5-m wind direction; (d) energy budget components, including net radiation Q^* , ground heat flux Q_G , sensible heat flux Q_H , and latent heat flux Q_E ; (e) energy balance residual $Q^* + Q_G + Q_E + Q_H$; and (f) 0–30-m bulk Richardson number. Vertical gray lines indicate the onset and cessation times of the temperature rise at

the stable slope layer. The increase in sensible heat flux is associated with the mixing out of the shallow stable surface layer over the slope. This mixing is responsible for the near-surface warming of air temperature. The warming of the surface leads to an increase in outgoing longwave radiation (i.e., a decrease in net radiation Q^*) and an increase in radiative cooling. The increase in downward turbulent sensible heat flux efficiently transports the cold air upward and reestablishes the nighttime decrease in near-surface air temperature.

The imbalance in the surface heat budget, represented by the nonzero sum of the energy budget components, is plotted in Fig. 7e. Such imbalances are a feature of many recent experiments over both homogeneous and complex topography and have been reported, for example, by Foken and Oncley (1995), Wilson et al. (2002), Weber and Kuttler (2005), and Oncley et al. (2007). The imbalance is negative during the cooling phase and rises to zero or positive numbers during the warming phase. This is a consistent feature of all warming events in the Owens Valley that we have investigated. The negative–positive imbalance seems to reflect the cooling–warming across the layer in which the measurements were taken. Its origin may be related to advective effects or to sensible and radiative heat flux divergences occurring between the surface and the levels of the sensible heat flux (5 m) and radiation (2 m) measurements.

Finally, the bulk Richardson number, as calculated from temperatures and wind velocities between the surface and the 30-m level, is shown in Fig. 7f. The Richardson number is above the critical value of 0.25 during the cooling phase, suggesting that turbulence is suppressed but falls below the critical Richardson number once the shear increases during the warming phase.

The 5-min-average time series data from selected levels of the towers was shown in Fig. 7. In this section, we present complementary data in the form of 5-min-average wind and temperature profiles from the towers. Figure 8 shows profiles taken just before (2035 PST) and just after (2115 PST) the temperature rises. A cold-air layer had developed over the slope (Fig. 8a) before the warming episode, with the bulk of the temperature deficit confined to the layer below 15 m. Background winds over the slope (Fig. 8b) had decreased from their afternoon values (4 m s^{-1} at 5-m height, as shown in Fig. 7b) and turned from downvalley into a downvalley–downslope direction (Figs. 7c, 8c). Wind speeds were about 2 m s^{-1} at the top of the tower, so vertical wind

← the central tower site. The dot–dash line in (b) marks the background wind speed increase. The alongvalley direction is shown in (c) by a horizontal gray line.

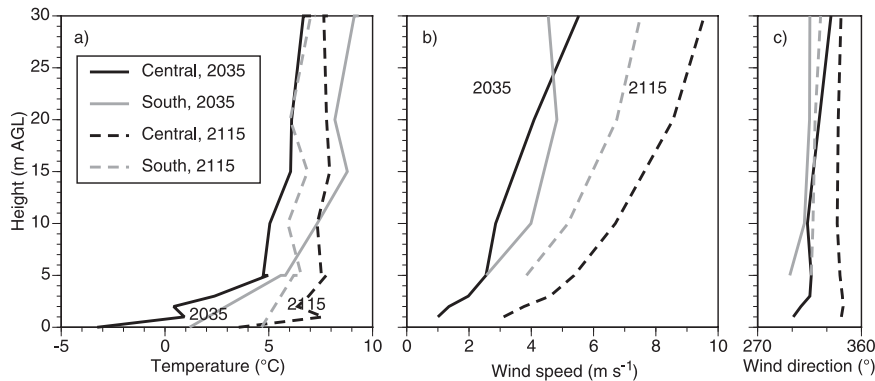


FIG. 8. Five-min-average central (black) and south (gray) tower (a) temperature, (b) wind speed, and (c) wind direction profiles at 2035 (solid) and 2115 (dashed) PST 17 Apr 2006. Sonic and aspirated temperature sensor measurements are shown in the temperature profiles as well as the effective radiating temperature at the surface. Sonic temperatures in (a) have not been corrected for their minor offsets from the adjacent aspirated temperature sensors.

shear across the tower layer was weak. During the warming episode, however, the background winds at the top of the tower (Fig. 8b) increased to 7–10 m s⁻¹, producing vertical shear across the shallow stable layer and mixing it out, causing air temperatures to rise at the central tower (Fig. 8a). At the south tower, the surface and near-surface temperature increase by 2115 PST was accompanied by a decrease of temperature above 5 m, probably caused by cold air mixed upward from the surface and horizontal cold-air advection.

To summarize, the 17 April case study shows a weakening of near-surface wind speed and a shift of winds from downvalley to downslope in a layer of radiatively cooled air over the slope. These slope flows advect cold-air downslope within the initially near-neutral valley atmosphere, causing the near-surface air temperatures to cool along the slope and eventually in the center of the valley. This cold-air layer reduces the surface friction felt by the background winds, which can thus accelerate. The warming episode begins when the increase in the background downvalley wind speed produces enough vertical shear across the downslope flow layer to trigger the turbulent mix out of the shallow stable layer over the slope. The mixing connects the flow near the ground with that aloft and turns the wind from its downslope direction more into the wind direction of the background flow. It should be pointed out that this day exhibited a daytime downvalley wind. Valley wind theory (Wagner 1938; Whiteman 1990, 2000) calls for thermally driven upvalley winds during daytime on undisturbed days. The daytime winds in this valley on 17 April were disturbed by strong winds aloft that were channeled along the valley axis, and the return to downvalley winds at night cannot be unambiguously attributed to either channeled winds or thermally driven down-

valley winds. The next case study will consider the sequence of events when background winds within the valley blow in the opposite direction (i.e., upvalley).

b. 19 April 2006

On 19 April, only a few of the HOBO sites (W07, V01–07 and V10) had warmings with $A \geq 0.75^\circ\text{C h}$. These sites included V02 and V03, which were the closest HOBO sites to the south and central towers, respectively.

The 19 April tower data from the central and south sites are shown in Fig. 9. On this date, a temperature rise of 5.0°C occurred at the central tower over a period of 0.92 h, and two warmings occurred at the south tower, with a temperature rise of 2.8°C (Fig. 9a) in the second warming, which occurred over a 0.25-h period. The temperature rise areas exceeded 0.75°C h at the surface at both sites and at the 1-, 2-, 3-, and 5-m levels of the central tower and at the 10- and 20-m levels at the south tower. The afternoon wind speeds (Fig. 9b) were above 4 m s^{-1} at both towers just before sunset, but the wind speeds, as in the previous case study, decreased near and after sunset. This case study differed from the previous one in that the afternoon wind was blowing up rather than down the valley (Fig. 9c). Once the wind speed fell below about 2 m s^{-1} , both valley floor tower sites experienced alternating downslope flows coming off the two opposing sidewalls. The westerly downslope flow from the Sierra Nevada occurred first because of the earlier local sunsets on the sierra slope. The warming episode was initiated with an acceleration of the upvalley wind. This turned the 5-m winds on the towers, so that they had both upvalley and downslope components. The south tower experienced two temperature rise episodes; each had a wind speed increase associated with them. Increases in sensible heat flux (Fig. 9d) were associated with the increases in

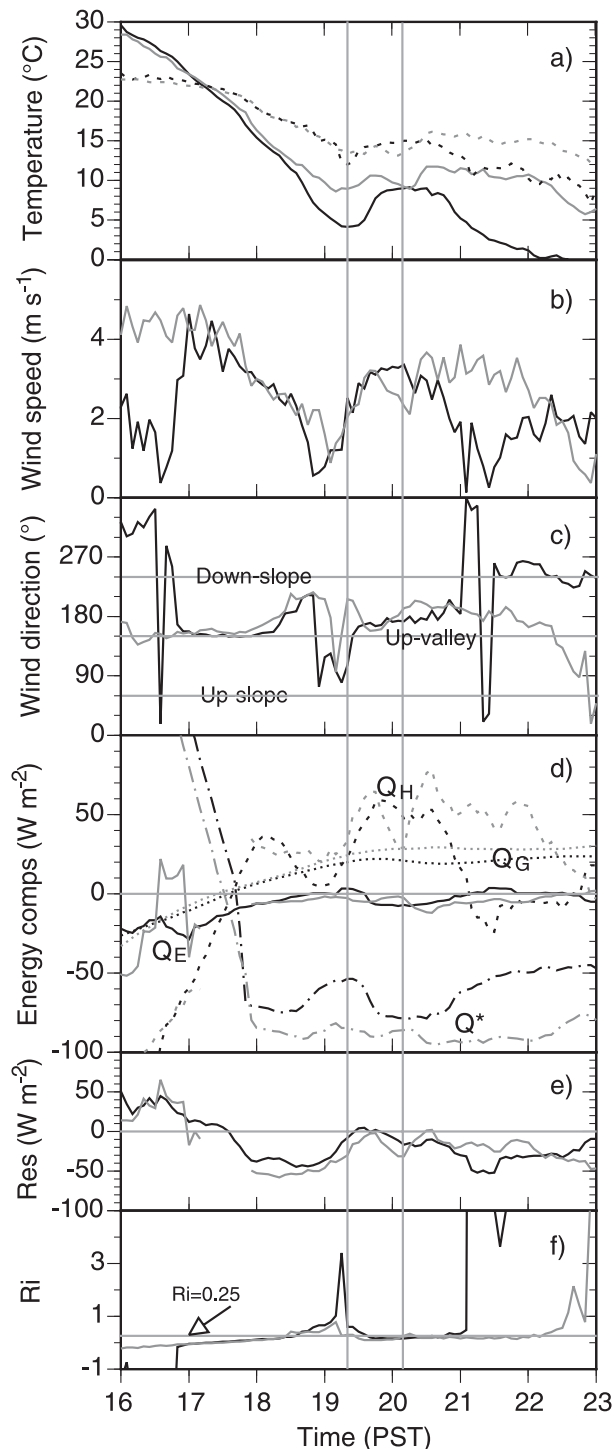


FIG. 9. As in Fig. 7, but for 19 Apr 2006.

wind speed that marked the temperature rises. Energy budget residuals (Fig. 9e) showed deficits during the cooling periods and near-balances during the warming episodes. The 0–30-m bulk Richardson number (Fig. 9f) was less than the critical value of 0.25 during the after-

noon; it rose above 0.25 as the winds decreased following sunset and dropped below 0.25 during the warming episodes, as in the previous case study. Like the previous case study, the stability in the tower layer (not shown) was relatively low during the afternoon cooling phase ($+5^{\circ}\text{C}$ in the 0–30-m-deep tower layer at 1815 PST), high during the period just before the warming episode began (8.5°C at the south tower and 12.5°C at the central tower at 1915 PST), and low again during the warming episode (6° – 7.5°C at 2000 PST) when the shallow layer of cold air was mixed out by the increasing turbulence.

c. 24 April 2006

On 24 April, only three HOBO sites—W01, V03 and V05—had $A \geq 0.75$. The 24 April tower data are shown in Fig. 10. The background wind direction within the valley was upvalley, as on 19 April. On this date, a 4°C warming occurred at the surface at the central tower over a 0.33-h period, and a 1.9°C warming occurred at the south tower over a 0.33-h period (Fig. 10a). The warming at south tower was poorly defined at the 5-m level of the tower, indicating that the phenomenon, despite its clear expression at the surface, was quite shallow. The warming episodes at both towers started after sunset when the 5-m wind speeds dropped below 2 m s^{-1} (Fig. 10b). The progression of events at the two towers was similar to the previous case studies. Wind speeds decreased rapidly after sunset to levels below 2 m s^{-1} , and the warming episodes began when the winds accelerated, reaching wind speeds of 3 m s^{-1} at 5 m. This case study illustrates that shallow inversions can be disturbed and mixed out with relatively light winds. A distinct shift in wind direction from upvalley to downslope initiated the central tower event (Fig. 10c), while the short-lived temperature rise at the south tower was initiated when weak upvalley winds shifted to downvalley and increased in speed. The downward turbulent sensible heat fluxes increased with vertical speed shear during the warming phase (Fig. 10d). The energy budget residual behaved as in the previous two case studies (Fig. 10e), and the Richardson number decreased to levels near or below 0.25 at the beginning of the warming phase (Fig. 10f), as in the previous two case studies. Like the 17 and 19 April cases, the mixing out of the shallow temperature deficit layer was well marked in the vertical temperature profiles (not shown).

7. Discussion

a. Sequence of events

The initial fall, the subsequent evening rise, and the reestablishment of the nighttime decline of near-surface temperatures on the sloping sidewall surfaces of the

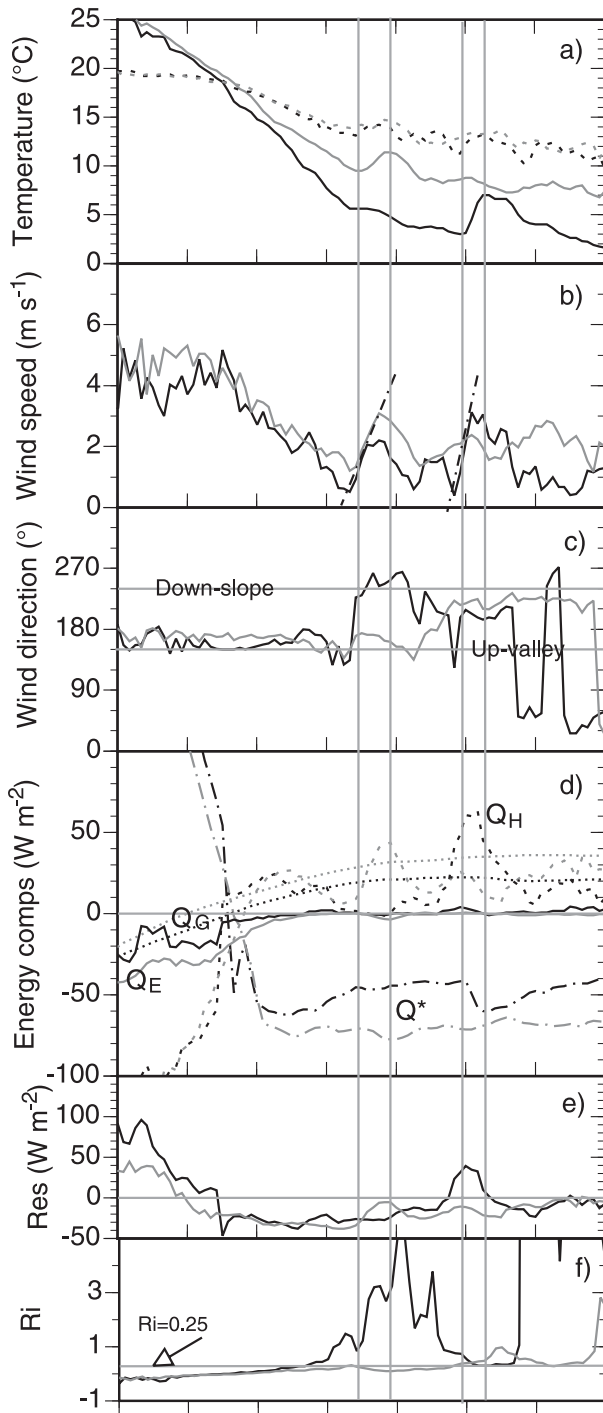


FIG. 10. As in Fig. 7, but for 24 Apr 2006. The onset and cessation times of the temperature rises are indicated by vertical gray lines for both the central and south sites.

Owens Valley are produced by a distinctive series of events, which will be summarized in this section.

Air and surface radiating temperatures fall in late afternoon as the sun gets lower in the sky and finally sets

behind the Sierra Nevada. An increase of the air cooling rate is observed when the net shortwave gain drops below the net longwave radiative loss (i.e., Q^* becomes negative). The ground surface cools more quickly than the adjacent air and a shallow, stably stratified air layer forms above the surface. The weak downward sensible heat flux in the stably stratified layer is not, on its own, strong enough to compensate for the cooling of the ground. The rapid fall of surface temperature is arrested, though, by the delayed addition of an upward flux of heat from the ground. Shear at the top of the cold air layer as well as longwave radiative flux divergence (André and Mahrt 1982) are possible causes of the thickening of the cold-air layer with time. The statically stable layer over the slope can form and remain intact if the background winds are not too strong. Even with moderate winds, an incipient stable layer can decouple the background winds from the surface, reducing wind speeds within the stable layer. The slope layer, being colder than the air at the same elevation adjacent to the slope, begins to move downhill because of its negative buoyancy. Acceleration of the downslope flow and the entrainment of ambient air at its top is another mechanism for the growth in depth of the layer (Manins and Sawford 1979). Because of this buoyancy-driven flow, the measured near-surface winds shift into a downslope direction or develop a downslope component. In a typical valley, this would result in air-flow perpendicular to the valley axis. The air in the shallow slope layer continues to cool radiatively during this phase. Additional cooling of this layer from the ground is required to maintain the negative buoyancy that allows the flow to continue against restraining and counterbalancing terms in both the momentum and heat budget equations (Haiden and Whiteman 2005).

A *warming episode* is initiated when prevailing or background winds above the statically stable downslope flow layer accelerate. The acceleration is a consequence of the submersion of frictional elements on the slopes and floor of the valley in the shallow stable layer, decoupling the background flows from the frictional influence of the underlying rough terrain. The acceleration increases the shear across the layer to the point at which the critical Richardson number is reached and turbulence in the layer is no longer suppressed. Turbulence mixes the layer, so that temperatures near the ground increase while temperatures at the top of the layer decrease. This near-ground air temperature increase produces the warming episode. The lower stability and enhanced vertical mixing allow momentum to be mixed downward into the layer, causing the downslope flows to be turned closer to the direction of the prevailing winds aloft, which are generally stronger than the weak downslope winds within the layer. The warming

at the surface increases the rate of longwave loss, reestablishing the general nighttime temperature decrease. The subsequent buildup of a deeper stable layer, especially over the valley floor, tends to isolate the valley floor from subsequent major mixing events, although smaller-scale temperature oscillations can still be generated within the stable layer.

Several of the steps leading to the warming scenario that we have described in mountain valleys have been hypothesized by previous investigators in connection with intermittent turbulence in stable boundary layers (SBLs) that form in the evening over horizontally homogeneous ground. Businger (1973), for example, considered that stability would increase rapidly at the surface in the evening as a result of strong radiative cooling and that the increase in stability would increase the Richardson number and suppress and collapse turbulence. The air above the SBL would be decoupled from the surface, and the lowered friction would cause it to accelerate, increasing the shear across the surface layer, causing the Richardson number in the layer to decrease and causing the SBL to break again into turbulence. He and others (e.g., Acevedo and Fitzjarrald 2001; van de Wiel et al. 2002) envisioned a cyclical process that would lead to a succession of intermittent turbulent episodes and oscillations in temperature and wind speed at the surface. In the Owens Valley, a variation of this mechanism appears to be responsible for the generation of the warming episodes, with the additional complication of drainage flows developing within the shallow stable boundary layer and wind accelerations developing in background winds that are channeled or driven thermally along the valley axis. These background winds accelerate when the shallow temperature deficit layer decouples the background flows from surface drag.

The variable times of the warming episodes from site to site and from day to day reflect the varying times required for the background flows adjacent to the slope to accelerate sufficiently to erode the cold-air layer. The background or prevailing winds in valleys most often flow along the valley's axis, normal to the direction of the downslope flows (Whiteman 2000). Such winds may be either channeled or thermally driven. In the case studies above, the winds were not thermally driven, as they do not undergo the normal day–night reversal of direction from upvalley to downvalley.

Warming episodes occurred frequently in the Owens Valley during the largely disturbed 60-day period of the T-REX experimental period when thermally driven and diurnally reversing valley flows were usually not in evidence. This illustrates that the warming episodes can occur with any prevailing wind direction. In the special case of pure thermally driven winds, the valley wind re-

versal normally goes through several stages (Defant 1949, 1951). First, after downslope winds begin, the daytime upvalley winds decelerate. Second, during the brief period when the upvalley winds die, the downslope winds exist on the slopes in a pure form. Third, in the presence of continued downslope winds, downvalley winds are initiated and increase in strength. Although we do not have an undisturbed T-REX period with pure thermally driven flows (i.e., without a background prevailing wind), we speculate that warming episodes will be seen in other valleys, even in cases with weak background flows. In these cases, the warming events could be initiated during the evening acceleration phase of the downvalley winds.

b. Micrometeorological aspects

Downslope flows and the temperature deficit layer in which they form are known to be quite sensitive to underlying topography and to changes in the atmospheric and surface variables that affect components of the surface energy balance (Whiteman 2000). Given our postulated mechanism for the evening warming, the magnitude of the temperature rises, and their timing will depend on the depths and strengths of the temperature deficit layers above individual sites. These depend on the topology of the top of the temperature deficit layer, which is affected by confluences and diffluences of the downslope flowing layer as its motion responds to the underlying topography. In the Owens Valley, evening temperature rises are not commonly seen on the steep east and upper west sidewalls and on surfaces that are convex (e.g., the ridgeline at the uppermost two or three datalogger sites on the upper west and Manzanar lines), but they are commonly encountered on the less steep alluvial fan of the lower west sidewall and in concave declivities on the sidewalls (middle Manzanar line) and at lower elevations in the valley (the valley line) where cold air tends to build up. Special topographic situations can enhance the strength and depth of the temperature deficit layer. For example, the highest frequency of warming episodes in our observation network was at W01, where a cold-air pond formed uphill of an irrigation ditch dike, and at M10, where air converges from higher elevations into the upper end of a broad, shallow valley. Additionally, warmings were less frequent and less intense at the west tower than at the central and south towers because the west tower was located on a small hill.

On the basis of the Owens Valley findings, we anticipate that such warming episodes will be found in temperature time series on the slopes of other valleys on clear nights, especially those in arid or semiarid environments with strong radiation climates where a nighttime cold-air layer develops readily over the valley floor and sidewalls.

c. Energy budget imbalance

An intriguing finding of this research is that the cooling of the slope flow layer is associated with negative energy budget imbalances. These imbalances largely disappear or reverse sign at the beginning of the warming phase, when shear produces turbulence that extends downward below the 5-m height where sensible heat flux was measured. The energy balance failure appears to be related to the lack of consideration of the full air volume between the ground and the 5-m level. The effects of the combined (and interacting) divergences of radiative and sensible heat flux between the surface and the 5-m level, and the effects of advection in the slope flow layer below the 5-m level may be responsible for the imbalance, which could be investigated using these data in future work.

d. Evening warmings at other locations

It is worth emphasizing the many possible causes of evening warmings in temperature traces over any type of topography. Inspection of temperature records over both flat and complex terrain will find warmings produced by a variety of meteorological processes, including advection (Lyons and Steedman 1981), cloud cover variations, wind break-ins, and short-term variations in variables that affect components of the surface energy balance. In mountain areas, oscillations in drainage flows and temperatures are well known (see section 4 for references). Foehn break-ins and other mechanisms that can produce warming events have been summarized by Geiger (1965). Turbulent erosion of a valley or basin inversion is another mechanism (Steinacker et al. 2007). Periodic cold-air avalanches (with intervening warmings) have also been noted in mountainous terrain (Kuettner 1949), as have nighttime warmings seen in thermograph recordings in Cochiti Canyon, New Mexico, that were believed to be “associated with air drainage and mountain-valley breezes which spring up during the night and for varying periods of time wipe out the usual nighttime valley inversions” (Von Eschen 1960). The emphasis of this paper is on the regular evening warmings on the floor and sidewalls of the broad Owens Valley, for which the interactions between shallow drainage flows and ambient flows within the bulk of the valley atmosphere become important.

8. Conclusions

The normal late afternoon or early evening temperature declines that occur at sites on the valley floor and sidewalls of California’s Owens Valley are often followed by short-lived evening temperature rises. The normal slow nighttime fall of temperature ensues after the evening temperature rise, although this cooling is

sometimes disturbed by short-term temperature excursions associated with slope flow oscillations. The distribution of the temperature rises in space and time over a 67-day period was investigated using a temperature datalogger network. Rises were most frequent at the valley floor center and at altitudes up to several hundred meters above the valley center on the west sidewall. The steeper, largely unvegetated east sidewall had fewer, not as well-developed rises. Rises were not in evidence when the valley atmosphere was well mixed by strong winds. On some nights, rises were found at many sites. The rises formed and decayed at about the same time at all sites. Case studies were pursued using data from heavily instrumented 34-m towers, and hypotheses were developed and tested to explain the phenomenon.

The temperature rises occurred with the breakdown of a shallow stable layer that formed over the valley slopes and floor following sunset. The formation of this layer was indicated by a turning of near-surface winds into the downslope direction as the flow accelerated down the slope as a result of the layer’s negative buoyancy. The temperature rises were produced by an acceleration of the background flow above the shallow temperature deficit layer on the slope, presumably caused by the decrease in surface friction felt by the background flow as the cold-air layer formed over the topography. The acceleration increased the vertical wind shear through the temperature deficit layer, decreased the bulk Richardson number to the critical level, and resulted in an onset of turbulence that mixed out the shallow slope layer, increasing the temperature of the near-surface air.

Acknowledgments. This research was supported by National Science Foundation (NSF) Grant ATM-0521776. SWH was supported by Swiss National Science Foundation Fellowship PBEZ2-113920. We thank Greg West, Jim Steenburgh, Hal Klieforth, and Johanna Whiteman for helping with the installation and retrieval of temperature dataloggers in Owens Valley, and Jonathan Wofsy and Maura Hahnenberger for their data analysis assistance. We thank Dr. Peggy Lemone at NCAR for references to previous relevant work. NCAR personnel at the Earth Observing Laboratory installed, operated, and processed data from the instrumented towers. Data were downloaded from the T-REX data archive, which is maintained by NCAR, which is supported by NSF.

REFERENCES

- Acevedo, O. C., and S. R. Fitzjarrald, 2001: The early evening surface-layer transition: Temporal and spatial variability. *J. Atmos. Sci.*, **58**, 2650–2667.

- André, J. C., and L. Mahrt, 1982: The nocturnal surface inversion and influence of clear-air radiative cooling. *J. Atmos. Sci.*, **39**, 864–878.
- Barr, S., and M. M. Orgill, 1989: Influence of external meteorology on nocturnal valley drainage winds. *J. Appl. Meteor.*, **28**, 497–517.
- Businger, J. A., 1973: Turbulent transfer in the atmospheric surface layer. *Workshop on Micrometeorology*, D. A. Haugen, Ed., Amer. Meteor. Soc., 67–98.
- Defant, F., 1949: Zur Theorie der Hangwinde, nebst Bemerkungen zur Theorie der Berg- und Talwinde (A theory of slope winds, along with remarks on the theory of mountain winds and valley winds). *Arch. Meteor. Geophys. Bioklimatol.*, **1A**, 421–450. [For English translation see Whiteman, C. D., and E. Dreiseitl, 1984: *Alpine Meteorology: Translations of Classic Contributions by A. Wagner, E. Ekhart, and F. Defant*, Pacific Northwest Laboratory, 97–121.]
- , 1951: Local winds. *Compendium of Meteorology*, T. M. Malone, Ed., Amer. Meteor. Soc., 655–672.
- Doran, J. C., 1991: The effects of ambient winds on valley drainage flows. *Bound.-Layer Meteor.*, **55**, 177–189.
- , and T. W. Horst, 1981: Velocity and temperature oscillations in drainage winds. *J. Appl. Meteor.*, **20**, 361–364.
- Foken, T., and S. Oncley, 1995: Workshop on instrumental and methodical problems of land surface flux measurements. *Bull. Amer. Meteor. Soc.*, **76**, 1191–1193.
- Geiger, R., 1965: *The Climate near the Ground*. Harvard University Press, 611 pp.
- Grubišić, V., and Coauthors, 2008: The Terrain-Induced Rotor Experiment: A field campaign overview including observational highlights. *Bull. Amer. Meteor. Soc.*, **89**, 1513–1533.
- Haiden, T., and C. D. Whiteman, 2005: Katabatic flow mechanisms on a low-angle slope. *J. Appl. Meteor.*, **44**, 113–126.
- Kuettner, J., 1949: Periodische Luftlawinen (Periodic air avalanches). *Meteor. Rundsch.*, **2** (5–6), 183–184.
- Lyons, T. J., and R. K. Steedman, 1981: Stagnation and nocturnal temperature jumps in a desert region of low relief. *Bound.-Layer Meteor.*, **21**, 369–387.
- Manins, P. C., and B. L. Sawford, 1979: A model of katabatic winds. *J. Atmos. Sci.*, **36**, 619–630.
- Monti, P., H. J. S. Fernando, M. Princevac, W. C. Chan, T. A. Kowalewski, and E. R. Pardyjak, 2002: Observations of flow and turbulence in the nocturnal boundary layer over a slope. *J. Atmos. Sci.*, **59**, 2513–2534.
- Oncley, S. P., and Coauthors, 2007: The Energy Balance Experiment EBEX-2000. Part I: Overview and energy balance. *Bound.-Layer Meteor.*, **123**, 1–28.
- Porch, W. M., R. B. Fritz, R. L. Coulter, and P. H. Gudiksen, 1989: Tributary, valley and sidewall air flow interactions in a deep valley. *J. Appl. Meteor.*, **28**, 578–589.
- Steinacker, R., and Coauthors, 2007: A sinkhole field experiment in the eastern Alps. *Bull. Amer. Meteor. Soc.*, **88**, 701–716.
- Stone, G. L., and D. E. Hoard, 1989: Low-frequency velocity and temperature fluctuations in katabatic valley flows. *J. Appl. Meteor.*, **28**, 477–488.
- Tyson, P. D., 1968: Velocity fluctuations in the mountain wind. *J. Atmos. Sci.*, **25**, 381–384.
- van de Wiel, B. J. H., R. J. Ronda, A. F. Moene, H. A. R. de Bruin, and A. A. M. Holtslag, 2002: Intermittent turbulence and oscillations in the stable boundary layer over land. Part I: A bulk model. *J. Atmos. Sci.*, **59**, 942–958.
- van Gorsel, E., 2003: Aspects of flow characteristics and turbulence in complex terrain. Ph.D. dissertation, University of Basel, 58 pp.
- Von Eschen, G. F., 1960: Nighttime temperature rises in mountain canyons. *Mon. Wea. Rev.*, **88**, 70–71.
- Wagner, A., 1938: Theorie und Beobachtung der periodischen Gebirgswinde (Theory and observation of periodic mountain winds). *Gerlands Beitr. Geophys.*, **52**, 408–449. [For English translation see Whiteman, C. D., and E. Dreiseitl, 1984: *Alpine Meteorology: Translations of Classic Contributions by A. Wagner, E. Ekhart, and F. Defant*, Pacific Northwest Laboratory, 13–43.]
- Weber, S., and W. Kuttler, 2005: Surface energy balance characteristics of a heterogeneous urban ballast facet. *Climate Res.*, **28**, 257–266.
- Whiteman, C. D., 1990: Observations of thermally developed wind systems in mountainous terrain. *Atmospheric Processes over Complex Terrain, Meteor. Monogr.*, No. 45, Amer. Meteor. Soc., 5–42.
- , 2000: *Mountain Meteorology: Fundamentals and Applications*. Oxford University Press, 355 pp.
- , J. M. Hubbe, and W. J. Shaw, 2000: Evaluation of an inexpensive temperature datalogger for meteorological applications. *J. Atmos. Oceanic Technol.*, **17**, 77–81.
- Wilson, K., and Coauthors, 2002: Energy balance closure at FLUXNET sites. *Agric. For. Meteorol.*, **113**, 223–243.